

# Structure and Properties of the Crystals of Solid Electrolytes (ZrO<sub>2</sub>)<sub>1-x-y</sub>(Sc<sub>2</sub>O<sub>3</sub>)<sub>x</sub>(Y<sub>2</sub>O<sub>3</sub>)<sub>y</sub> (x = 0.035–0.11, y = 0–0.02) Prepared by Selective Melt Crystallization<sup>1</sup>

M. A. Borik<sup>a</sup>, S. I. Bredikhin<sup>b</sup>, V. T. Bublik<sup>c</sup>, A. V. Kulebyakin<sup>a</sup>, I. E. Kuritsyna<sup>b</sup>, E. E. Lomonova<sup>a</sup>,  
F. O. Milovich<sup>c</sup>, V. A. Myzina<sup>a</sup>, V. V. Osiko<sup>a</sup>, S. V. Seryakov<sup>c</sup>, and N. Yu. Tabachkova<sup>c</sup>, \*

<sup>a</sup>Prokhorov Institute of General Physics, Russian Academy of Sciences, ul. Vavilova 38, Moscow, Russia

<sup>b</sup>Institute of Solid State Physics, Russian Academy of Sciences,  
ul. Akademika Osip'yana 2, Chernogolovka, Moscow oblast, Russia

<sup>c</sup>National University of Science and Technology MISiS, Leninskii pr. 4, Moscow, Russia

\*e-mail: ntabachkova@gmail.com

Received July 27, 2015

**Abstract**—Single crystals of solid electrolytes of the (ZrO<sub>2</sub>)<sub>1-x-y</sub>(Sc<sub>2</sub>O<sub>3</sub>)<sub>x</sub>(Y<sub>2</sub>O<sub>3</sub>)<sub>y</sub> (x = 0.035–0.11, y = 0–0.02) system were grown by selective melt crystallization. Stabilization of ZrO<sub>2</sub> only with Sc<sub>2</sub>O<sub>3</sub> in the concentration range 9–11 mol % Sc<sub>2</sub>O<sub>3</sub> did not afford crystals with a cubic structure, and only the introduction of additional Y<sub>2</sub>O<sub>3</sub> stabilizers afforded uniform transparent single-phase cubic crystals. All the crystals under study had high microhardness, but low crack resistance. The ion conductivity of crystals with 6 and 9 mol % Sc<sub>2</sub>O<sub>3</sub> (6ScZr and 9ScZr, respectively) is comparable to that of 8 mol % Y<sub>2</sub>O<sub>3</sub>-stabilized ZrO<sub>2</sub> (8YSZ), which is the most suitable electrolyte in the ZrO<sub>2</sub>–Y<sub>2</sub>O<sub>3</sub> binary system. The specific conductivity of crystals containing 8–10 mol % Sc<sub>2</sub>O<sub>3</sub> and 1–2 mol % Y<sub>2</sub>O<sub>3</sub> exceeds that of other materials including 8YSZ. The maximum conductivity in the given range of compositions is inherent in the cubic phase with 10 mol % Sc<sub>2</sub>O<sub>3</sub> and 1 mol % Y<sub>2</sub>O<sub>3</sub> (10Sc1YZr).

**Keywords:** solid electrolytes, zirconia, single crystals, phase composition, structure, ion conductivity, mechanical properties

**DOI:** 10.1134/S1023193516070041

## INTRODUCTION

The materials based on zirconia stabilized with scandium and yttrium oxides are of great interest because they possess the highest ion conductivity among solid electrolytes based on ZrO<sub>2</sub>. The use of these materials allows the lowering of the working temperature of fuel cells to 800°C, which is rather important for increasing the stability, operational life, and reliability of electrochemical devices [1–6]. Solid electrolytes are used mainly in the form of gas-proof ceramic membranes. When materials are prepared in the form of single crystals, in contrast to ceramics, the role of grain boundary factors can be excluded. In particular, one of the problems for solid electrolytes is the stability of characteristics at working temperatures for a long time, which may be due to both phase transformations and high-temperature recrystallization of ceramics. For single crystals, the stability is determined only by the phase stability at working temperatures. One of the most attractive methods for growing

the crystals of oxide materials with high melting points is selective melt crystallization using direct high-frequency (HF) melting in a cold crucible [7–9].

The goal of this study was to prepare single crystals and study the phase composition, crystal structure, and properties of solid solutions of the (ZrO<sub>2</sub>)<sub>1-x-y</sub>(Sc<sub>2</sub>O<sub>3</sub>)<sub>x</sub>(Y<sub>2</sub>O<sub>3</sub>)<sub>y</sub> system (x = 0.035–0.11; y = 0–0.02).

## EXPERIMENTAL

The (ZrO<sub>2</sub>)<sub>1-x-y</sub>(Sc<sub>2</sub>O<sub>3</sub>)<sub>x</sub>(Y<sub>2</sub>O<sub>3</sub>)<sub>y</sub> single crystals were grown by selective melt crystallization in a water-cooled copper crucible with a diameter of 130 mm. The crystals were grown on a Kristall-407 unit (frequency 5.28 MHz, maximum output capacity 60 kW). The mass of the charge was 6 kg. To prepare the batch mixture, we used ZrO<sub>2</sub>, Sc<sub>2</sub>O<sub>3</sub>, and Y<sub>2</sub>O<sub>3</sub> powders (99.99%). Selective melt crystallization was performed by moving down the crucible with a melt relative to the inductor at a rate of 10 mm/h. The procedure gave ingots consisting of columnar crystals, which were mechanically separated into unit crystals. The XRD analysis was performed on a Bruker D8 X-ray diffrac-

<sup>1</sup> Published on the basis of the materials of III All-Russia Conference “Fuel Cells and Power Plants on Their Basis,” Chernogolovka, 2015.

**Table 1.** Composition of grown crystals

Crystal composition	Symbol	Description of crystals
$(\text{ZrO}_2)_{0.965}(\text{Sc}_2\text{O}_3)_{0.035}$	3.5ScZr	Nontransparent, with microcracks throughout the bulk
$(\text{ZrO}_2)_{0.94}(\text{Sc}_2\text{O}_3)_{0.06}$	6ScZr	Semi-transparent, with macrocracks
$(\text{ZrO}_2)_{0.91}(\text{Sc}_2\text{O}_3)_{0.09}$	9ScZr	Semi-transparent, without cracks
$(\text{ZrO}_2)_{0.89}(\text{Sc}_2\text{O}_3)_{0.11}$	11ScZr	Slightly opalescent, without cracks
$(\text{ZrO}_2)_{0.91}(\text{Sc}_2\text{O}_3)_{0.08}(\text{Y}_2\text{O}_3)_{0.01}$	8Sc1YZr	Semi-transparent (bottom) and transparent (top)
$(\text{ZrO}_2)_{0.90}(\text{Sc}_2\text{O}_3)_{0.09}(\text{Y}_2\text{O}_3)_{0.01}$	9Sc1YZr	Transparent and semi-transparent bands
$(\text{ZrO}_2)_{0.90}(\text{Sc}_2\text{O}_3)_{0.08}(\text{Y}_2\text{O}_3)_{0.02}$	8Sc2YZr	Completely transparent
$(\text{ZrO}_2)_{0.89}(\text{Sc}_2\text{O}_3)_{0.09}(\text{Y}_2\text{O}_3)_{0.02}$	9Sc2YZr	
$(\text{ZrO}_2)_{0.89}(\text{Sc}_2\text{O}_3)_{0.10}(\text{Y}_2\text{O}_3)_{0.01}$	10Sc1YZr	
$(\text{ZrO}_2)_{0.88}(\text{Sc}_2\text{O}_3)_{0.11}(\text{Y}_2\text{O}_3)_{0.01}$	11Sc1YZr	
$(\text{ZrO}_2)_{0.88}(\text{Sc}_2\text{O}_3)_{0.11}(\text{Y}_2\text{O}_3)_{0.01}$	11Sc1YZr	Semi-transparent (bottom) and transparent (top)

tometer ( $\text{CuK}_\alpha$  radiation) on the samples in the form of ground powders and crystals. The crystal structure was studied by transmission electron microscopy (TEM) using a JEM 2100 microscope (accelerating voltage 200 kV). For electron microscopy, the samples were polished to a thickness of 200  $\mu\text{m}$ . The sample was prepared by ion etching using a PIPS (Precision Ion Polishing System, Gatan) unit. The density was determined by hydrostatic weighing on a Sartorius instrument for hydrostatic weighing (the error was 0.05%). The microhardness of the crystals was determined on a DM 8 B AUTO microhardness tester.

The electric conductivity was studied in the temperature range 400–900°C using a Solartron SI1260 frequency analyzer in the frequency range 1 Hz–5 MHz with an amplitude of the AC signal of 24 mV. For measurements we used crystal plates with an area of  $7 \times 7 \text{ mm}^2$  and a thickness of 0.5 mm. To form current contacts, a platinum paste was applied to the opposite sides of the crystals; the paste was burned into the crystals at 950°C for 1 h in air.

**Table 2.** Density and microhardness of  $(\text{ZrO}_2)_{1-x-y}(\text{Sc}_2\text{O}_3)_x(\text{Y}_2\text{O}_3)_y$  crystals

Sample	Density, $\text{g/cm}^3$	Microhardness $H_V$ , $\text{kgF/mm}^2$	Load, g
3.5ScZr	$5.822 \pm 0.006$	$1240 \pm 40$	300
6ScZr	$5.868 \pm 0.006$	$1625 \pm 30$	300
9ScZr	$5.807 \pm 0.001$	$1590 \pm 40$	200
11ScZr	$5.722 \pm 0.001$	$1640 \pm 30$	100
8Sc1YZr*	$5.824 \pm 0.001$	$1425 \pm 40$	50
8Sc2YZr	$5.811 \pm 0.001$	$1530 \pm 50$	25
9Sc1YZr*	$5.769 \pm 0.005$	$1530 \pm 40$	100
9Sc2YZr	$5.760 \pm 0.001$	$1505 \pm 40$	50
10Sc1YZr	$5.744 \pm 0.001$	$1550 \pm 40$	50
10Sc2YZr	$5.741 \pm 0.002$	$1470 \pm 25$	100
11Sc1YZr*	$5.720 \pm 0.002$	$1480 \pm 30$	50

\* Transparent part.

## RESULTS AND DISCUSSION

Table 1 lists the compositions of the grown crystals, their description, and the notation used below. Figure 1 shows the view of semi-transparent and transparent crystals and the crystal with alternating transparent and semi-transparent regions.

All grown crystals had the shape and size similar to those of zirconia crystals partially stabilized with  $\text{Y}_2\text{O}_3$  and obtained by selective melt crystallization in a cold crucible [10, 11].

The 3.5ScZr and 6ScZr samples had cracks in the bulk of crystal after growth. The cracking of the crystals of these compositions is obviously explained by the phase transitions in the high-temperature range [12] and/or high thermomechanical stresses that appear on cooling. The additional introduction of  $\text{Y}_2\text{O}_3$  affords optically homogeneous transparent crystals without visible defects (8Sc2YZr, 9Sc2YZr, 10Sc1YZr, and 10Sc2YZr). This serves as indirect evidence for the results of [5, 13–16], which reported that additional introduction of cerium or yttrium oxides in the  $\text{ZrO}_2$ – $\text{Sc}_2\text{O}_3$  system increases the phase stability of cubic zirconia.

The densities and mechanical characteristics of the crystals are given in Table 2. The crystals have high microhardness and low crack resistance. The introduction of  $\text{Y}_2\text{O}_3$  necessitates a decrease in the maximum loads on the indenter at which the sample remains stable without cracking (the last column of Table 2). The microhardness was measured just at these loads.

The diffraction patterns of  $(\text{ZrO}_2)_{1-x}(\text{Sc}_2\text{O}_3)_x$  are shown in Fig. 2. The phase composition of the powder samples shows that 3.5ScZr consists of two phases: tetragonal and monoclinic, the main of which is the monoclinic phase. The diffraction patterns show only the lines of the tetragonal phase for 6ScZr and 9ScZr and the lines of the rhombohedral phase for 11ScZr. Figures 2b–2h show the regions of the diffraction patterns in the range of sixth order reflections from the

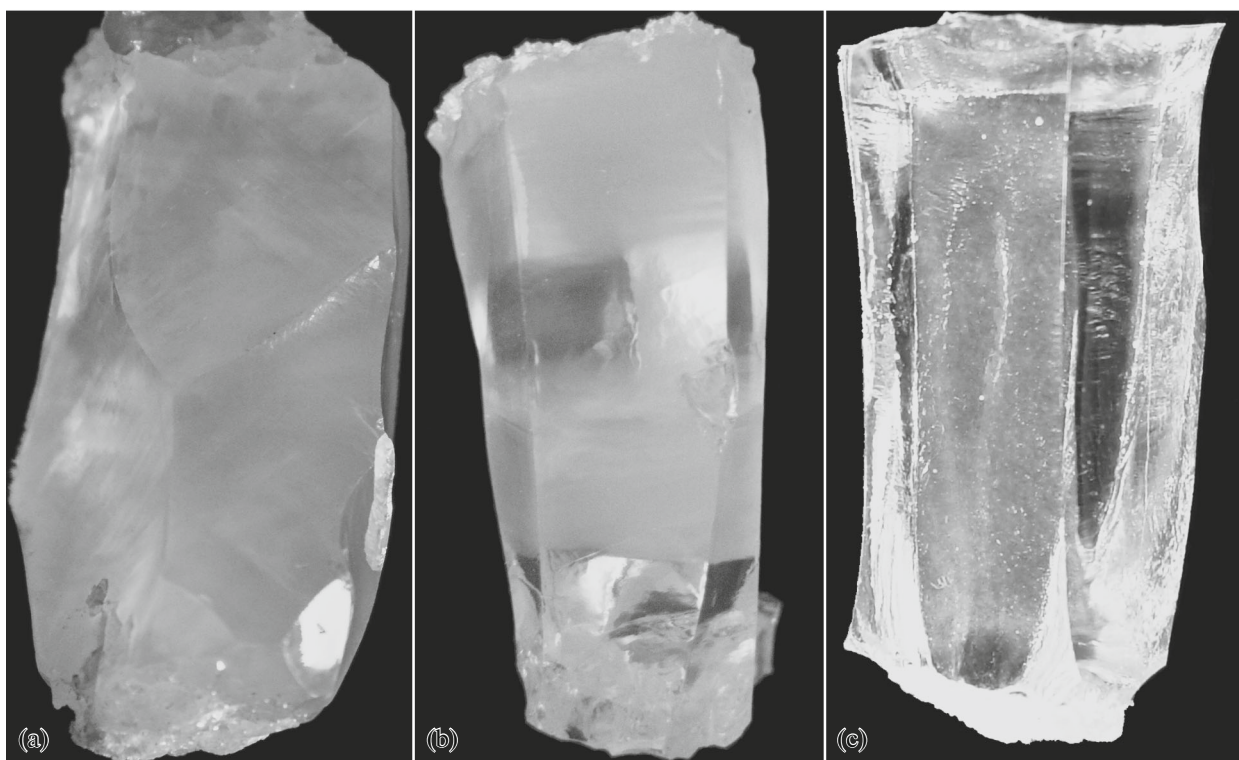


**Fig. 1.** View of the crystals: (a) semi-transparent, (c) transparent, and (b) with alternating transparent and semi-transparent regions.

(100) plane for the 3.5ScZr, 6ScZr, and 9ScZr crystals and third order reflections from the (012) plane for 11ScZr. The simultaneous appearance of the (006) and (600) diffraction maxima for the crystals orientated along the (100) plane is due to the twinning along the planes of {110} type. A comparison of the data on the crystals and powders prepared from the given crystals shows that the mechanical grinding of the samples did not lead to a change in the phase composition. In contrast to the  $(\text{ZrO}_2)_{1-x}(\text{Y}_2\text{O}_3)_x$  crystals, the tetragonal phase in the  $(\text{ZrO}_2)_{1-x}(\text{Sc}_2\text{O}_3)_x$  crystals is not liable to the tetragonal–monoclinic transition after mechanical treatment irrespective of the degree of tetragonality. This agrees with the results of [6], which reported that the cutting and polishing of the samples containing 4 mol %  $\text{Sc}_2\text{O}_3$  was not accompanied by a pronounced tetragonal monoclinic phase transition. The tetragonal phases in 3.5ScZr, 6ScZr, and 9ScZr had a low degree of tetragonality ( $c/a$ ), namely, 1.016, 1.012, and 1.007, respectively. As the concentration of  $\text{Sc}_2\text{O}_3$  in crystals increases, the degree of tetragonality decreases, their structure becoming close to cubic.

Importantly, in the samples with high  $\text{Sc}_2\text{O}_3$  contents (9ScZr and 11ScZr), there was no cubic phase. This disagrees with the results for ceramic synthesis at sintering temperatures of up to 1500°C [5, 6, 16–20]. A possible reason is the fact that the crystals under study were obtained from a melt and their thermal background differs considerably from that of the

ceramic samples. This is confirmed by the fact that the phase composition of the quenched molten polycrystalline samples corresponds to our data except for the samples with 18–20 mol %  $\text{ScO}_{1.5}$  (10–11 mol %  $\text{Sc}_2\text{O}_3$ ), in which traces of the cubic phase were found [21].

The phase composition of the  $(\text{ZrO}_2)_{1-x-y}(\text{Sc}_2\text{O}_3)_x(\text{Y}_2\text{O}_3)_y$  solid solutions of the crystals and powders prepared from these crystals is given in Table 3. It can be seen that 8Sc2YZr, 9Sc2YZr, and 10Sc1YZr do not experience a phase transition on grinding. For 8Sc1YZr and 9Sc1YZr, the phase composition for crystals and powders was the same. In 8Sc1YZr, only the tetragonal modification was pres-

**Table 3.** Phase composition of  $(\text{ZrO}_2)_{1-x-y}(\text{Sc}_2\text{O}_3)_x(\text{Y}_2\text{O}_3)_y$  crystals and powders

Sample	Phase composition of	
	crystals	powders
8Sc1YZr	<i>t</i>	<i>t</i>
8Sc2YZr	<i>c</i>	<i>c</i>
9Sc1YZr	<i>c + t</i>	<i>c + t</i>
9Sc2YZr	<i>c</i>	<i>c</i>
10Sc1YZr	<i>c</i>	<i>c</i>
10Sc2YZr	<i>c</i>	<i>c + r</i>
11Sc1YZr	<i>c + r</i>	<i>r + c</i>

Modifications of  $\text{ZrO}_2$ : *c* cubic; *t* tetragonal, and *r* rhombohedral.

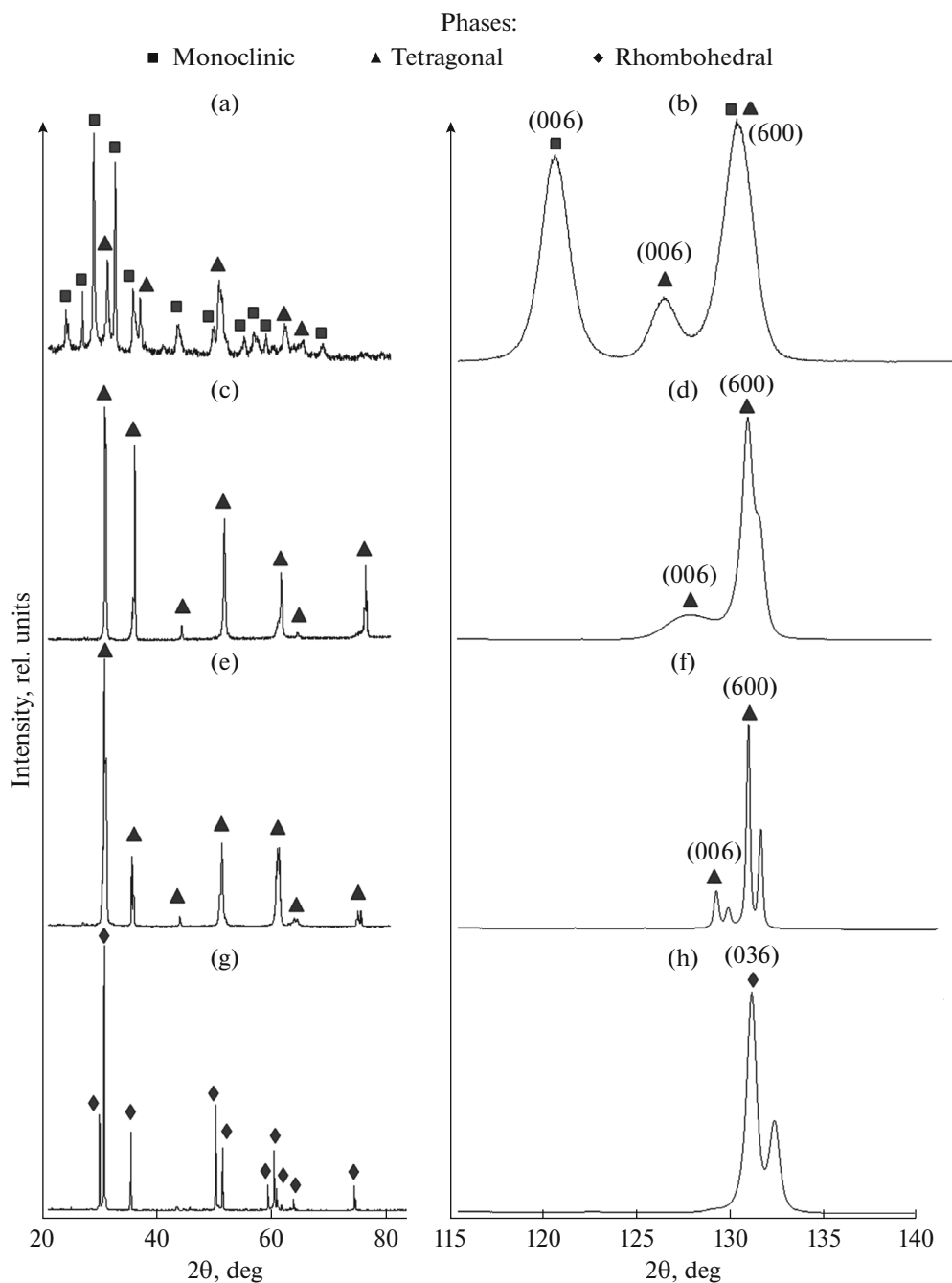


**Fig. 2.** Diffraction patterns of the (a, c, e, g) powder and (b, d, f, h)  $(\text{ZrO}_2)_{1-x}(\text{Sc}_2\text{O}_3)_x$  single-crystal samples: (a, b) 3.5ScZr; (c, d) 6ScZr; (e, f) 9ScZr; and (g, h) 11ScZr.

ent, while in 9Sc1YZr, the cubic phase was found along with the tetragonal phase. The phase composition changed on grinding only for 10Sc2YZr and 11Sc1YZr, where the cubic phase partially transformed into the rhombohedral phase, suggesting high degree of metastability.

Thus, the replacement of 1 mol %  $\text{Sc}_2\text{O}_3$  in the 9ScZr crystal by  $\text{Y}_2\text{O}_3$  (8Sc1YZr) did not lead to any change in the phase composition, though transparent

regions appeared in very small areas in the upper part of the crystal. The addition of another 1 mol %  $\text{Y}_2\text{O}_3$  allowed us to obtain 8Sc2YZr single crystals with a cubic structure, which was also preserved on grinding. The addition of 1 mol %  $\text{Y}_2\text{O}_3$  to the 9ScZr crystal led to the appearance of a cubic phase along with the tetragonal one in the 9Sc1YZr crystal; an increase in the  $\text{Y}_2\text{O}_3$  content to 2 mol % yielded cubic crystals. Note that the zirconia crystals stabilized with 10 mol %  $\text{Sc}_2\text{O}_3$

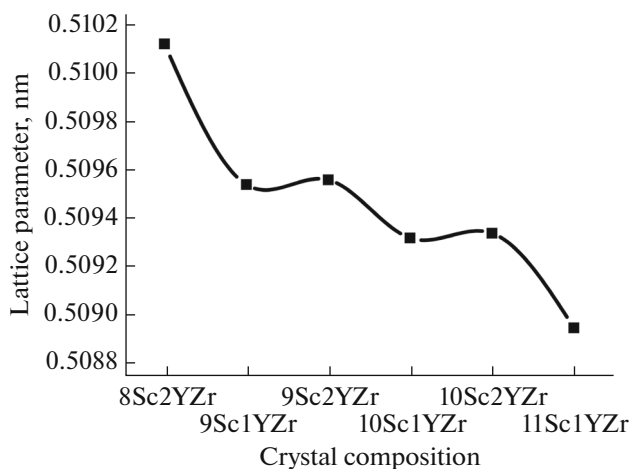
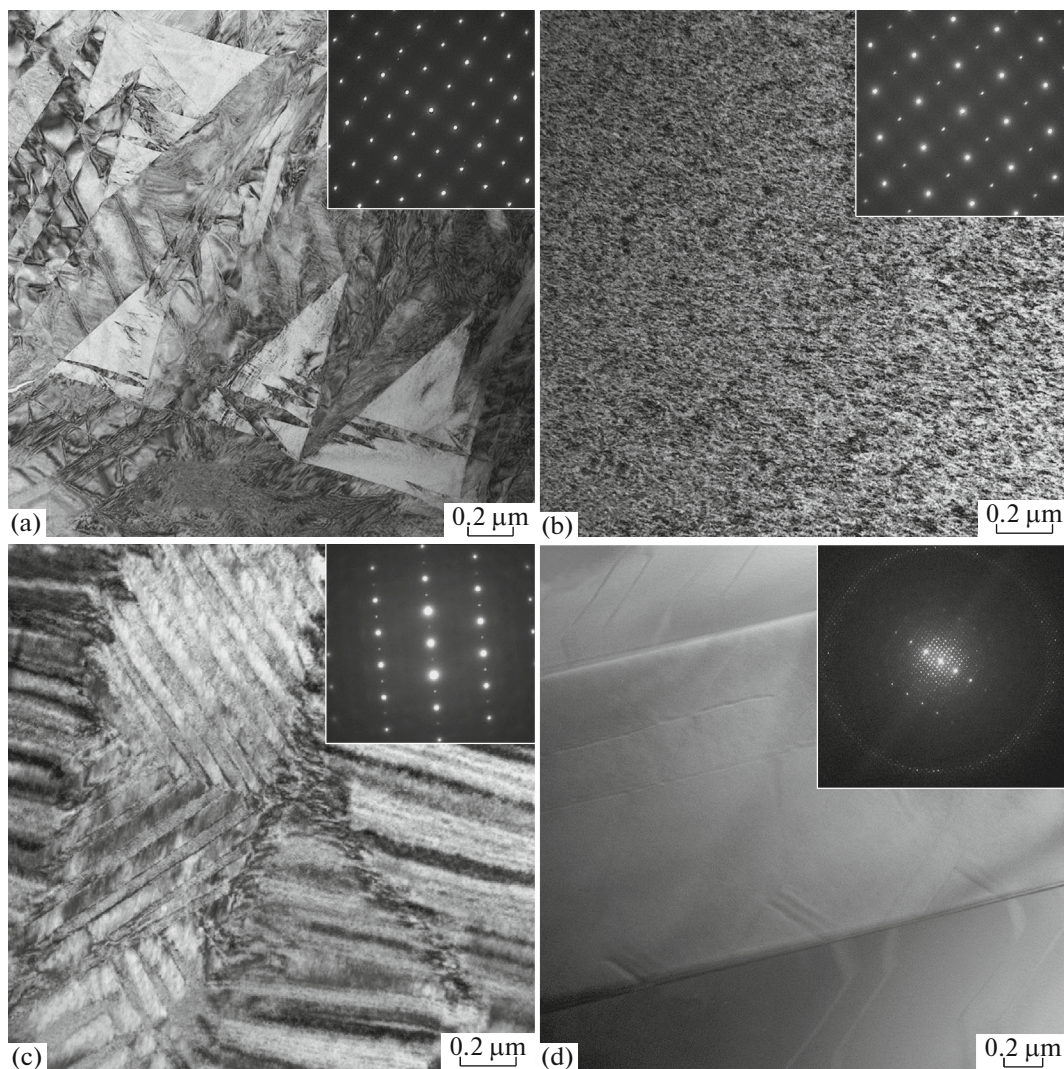


**Fig. 3.** Dependence of the lattice parameter of the cubic solid solutions  $(\text{ZrO}_2)_{1-x-y}(\text{Sc}_2\text{O}_3)_x(\text{Y}_2\text{O}_3)_y$  on the crystal composition.

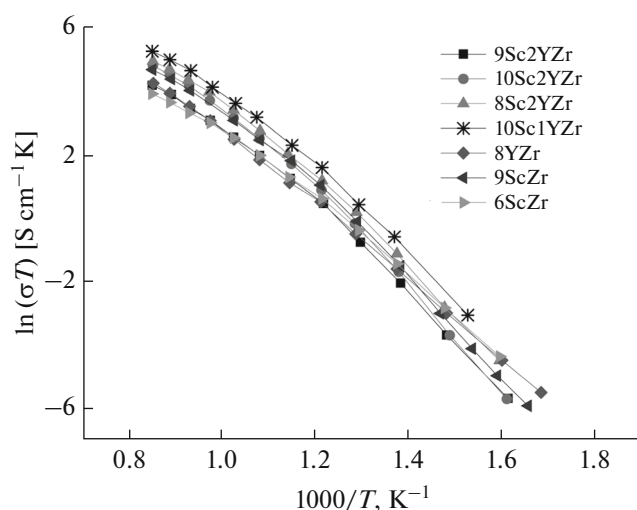
and 1 mol %  $\text{Y}_2\text{O}_3$  had a cubic structure, but an increase in the  $\text{Y}_2\text{O}_3$  content to 2 mol % led to the fact that the phase stability decreased and a rhombohedral phase appeared on grinding. This was also characteristic for 11Sc1YZr, in which semi-transparent regions were observed in the lower part of the crystals after growth.

Figure 3 shows a change in the lattice parameter in the cubic crystals of the  $(\text{ZrO}_2)_{1-x-y}(\text{Sc}_2\text{O}_3)_x(\text{Y}_2\text{O}_3)_y$  solid solutions. The cubic lattice constant decreases when the total concentration of the stabilizer oxide increases (from 10 to 12 mol %). The additional introduction of  $\text{Y}_2\text{O}_3$  slightly decreases this tendency due to the large ion radius of  $\text{Y}^{3+}$  relative to that of  $\text{Sc}^{3+}$ .

A transparent electron microscopy study showed that twins were present in  $(\text{ZrO}_2)_{1-x}(\text{Sc}_2\text{O}_3)_x$  crystals ( $x = 0.035-0.11$ ). The form and size of twins depend on the  $\text{Sc}_2\text{O}_3$  concentration (Fig. 4). The morphology



**Fig. 4.** TEM images of  $(\text{ZrO}_2)_{1-x}(\text{Sc}_2\text{O}_3)_x$  crystals: (a) 3.5ScZr, (b) 6ScZr, (c) 9ScZr, and (d) 11ScZr. Inserts: diffraction patterns from the corresponding regions of the crystals.



**Fig. 5.** Temperature dependences of specific conductivity of  $(\text{ZrO}_2)_{1-x-y}(\text{Sc}_2\text{O}_3)_x(\text{Y}_2\text{O}_3)_y$  crystals.

of the twin structure changed nonmonotonically as  $x$  increased. For 3.5ScZr, large needle twins were observed, which are characteristic for the monoclinic phase. For 6ScZr, the twin structure is quite homogeneous and finely disperse. The twinning in this sample was also confirmed by XRD data; this morphology of the twin structure was observed in  $(\text{ZrO}_2)_{1-x}(\text{Y}_2\text{O}_3)_x$  [22]. At increased  $\text{Sc}_2\text{O}_3$  concentration, the size of the twins in the 9ScZr sample increases. According to Fig. 4c, the primary twin plates of the crystal, in turn, are also twinned. The traces of the secondary twinning planes lie at an angle of  $\sim 45^\circ$  to the trace of the primary twinning plane. The largest twins were observed in the rhombohedral 11ScZr crystal. A study of cubic crystals stabilized with  $\text{Sc}_2\text{O}_3$  and  $\text{Y}_2\text{O}_3$  showed the absence of a twin structure, which generally forms during phase transitions on cooling [22].

The specific electric conductivity, primarily, oxygen-ion conductivity was calculated by analyzing the impedance spectra measured at a fixed temperature. The 3.5ScSZ and 11ScSZ samples were not studied

because of microcracks in the crystals and crystal decomposition during the preparation for measurements. Figure 5 shows the temperature dependences of conductivity. Two linear regions in Arrhenius coordinates can be isolated for each composition (623–823 K and 823–1173 K). Table 4 lists the ion conductivity activation energies ( $E_a$ ). For comparison, it also gives the data for the single crystals of the  $(\text{ZrO}_2)_{0.92}(\text{Y}_2\text{O}_3)_{0.08}$  solid solution (8YSZ) [23]. The presence of a fracture is explained by a change in the mechanism of ion transport on heating. According to the data of [24], in the low-temperature range,  $E_a$  is the sum of the association energy ( $E_{as}$ ) required for dissociation of the “oxygen vacancy–impurity cation” cluster and the migration energy ( $E_m$ ) of the mobile ions:

$$E_a = E_{as} + E_m. \quad (1)$$

In the high-temperature range, the first term is negligibly small, and the activation energy of conductivity is determined by  $E_m$ . According to estimations,  $E_{as}$  for the  $\text{ZrO}_2$ – $\text{Sc}_2\text{O}_3$  and  $\text{ZrO}_2$ – $\text{Sc}_2\text{O}_3$ – $\text{Y}_2\text{O}_3$  systems is  $\sim 0.33$ – $0.49$  eV and  $0.43$ – $0.53$  eV, respectively. The resulting values are comparable to  $E_{as}$  for  $\text{ZrO}_2$ – $\text{Y}_2\text{O}_3$  calculated in [23].

According to the obtained data, the ion conductivity of 6ScZr and 9ScZr crystals in the temperature range 673–973 K is comparable to that of 8YSZ crystals. In the temperature range 973–1173 K, the conductivity of the  $\text{ZrO}_2$ – $\text{Sc}_2\text{O}_3$  system is 1.5 times higher than that of 8YSZ, which has the maximum conductivity in the  $\text{ZrO}_2$ – $\text{Y}_2\text{O}_3$  system. Note that  $\text{ZrO}_2$ – $\text{Sc}_2\text{O}_3$  at 673–973 K has slightly higher  $E_a$  than  $\text{ZrO}_2$ – $\text{Y}_2\text{O}_3$ ; in the high-temperature range, the  $E_a$  values are comparable.

A comparison of the specific conductivities of cubic crystals stabilized with  $\text{Sc}_2\text{O}_3$  and  $\text{Y}_2\text{O}_3$  shows that the specific conductivity of 10Sc1YZr is higher than that of 8Sc2YZr, 9Sc2YZr, and 10Sc2YZr. For 8Sc2YZr and 10Sc2YZr, it is almost the same in the high-temperature range, while for 9Sc2YZr it is the lowest. The conductivity of these materials exceeds

**Table 4.** Activation energies and conductivities of  $(\text{ZrO}_2)_{1-x-y}(\text{Sc}_2\text{O}_3)_x(\text{Y}_2\text{O}_3)_y$  crystals

Material	$E_a$ , eV		Specific conductivity, $\text{S cm}^{-1}$			
	673–823 K	823–1173 K	973 K	1073 K	1123 K	1173 K
6ScZr	1.13	0.80	0.013	0.026	0.035	0.044
9ScZr	1.36	0.87	0.023	0.053	0.073	0.094
8YSZ	1.08	0.87	0.013	0.032	0.046	0.062
8Sc2YZr	1.29	0.86	0.032	0.074	0.100	0.123
9Sc2YZr	1.37	0.87	0.013	0.030	0.045	0.057
10Sc1YZr	1.30	0.85	0.040	0.100	0.134	0.168
10Sc2YZr	1.43	0.90	0.024	0.062	0.084	0.110

that of tetragonal 6ScZr and 9ScZr stabilized only with Sc<sub>2</sub>O<sub>3</sub> almost threefold.

The conductivity data obtained for the crystals proved higher than for the ceramic samples with similar compositions [5]. In addition, while the conductivity of ceramic 9Sc2YZr in the range 873–1273 K [5] is slightly higher than for 10Sc1YZr, on crystals studied here the conductivity of 10Sc1YZr is higher than for 9Sc2YZr. This suggests that it is important to take into account the intergrain effects, in particular, possible segregation of the stabilizing additions in the case of ceramic materials.

## CONCLUSIONS

The single crystals of the solid solutions of the (ZrO<sub>2</sub>)<sub>1-x-y</sub>(Sc<sub>2</sub>O<sub>3</sub>)<sub>x</sub>(Y<sub>2</sub>O<sub>3</sub>)<sub>y</sub> system were grown for the first time by selective melt crystallization. It was shown that the introduction of additional stabilizing oxide Y<sub>2</sub>O<sub>3</sub> allows one to grow homogeneous transparent single-phase cubic crystals. The range of compositions for growing the cubic crystals from a melt was determined:  $x = 0.08-0.11$ ;  $y = 1-0.02$ . Mechanical grinding of the samples did not change the phase composition of the (ZrO<sub>2</sub>)<sub>1-x</sub>(Sc<sub>2</sub>O<sub>3</sub>)<sub>x</sub> crystals. For (ZrO<sub>2</sub>)<sub>1-x-y</sub>(Sc<sub>2</sub>O<sub>3</sub>)<sub>x</sub>(Y<sub>2</sub>O<sub>3</sub>)<sub>y</sub>, the phase composition changed after grinding only for 10Sc2YZr and 11Sc1YZr, indicating that the stability of the cubic phase decreased.

It was shown that the (ZrO<sub>2</sub>)<sub>1-x</sub>(Sc<sub>2</sub>O<sub>3</sub>)<sub>x</sub> crystals have a twin structure of different types depending on the composition. The cubic crystals have no twin structure.

The crystals of the solid solutions under study have high microhardness, but low cracking resistance.

The ion conductivities of 6ScZr and 9ScZr crystals are comparable to the conductivity of 8YSZ, but higher in the temperature range 823–1173 K. Co-doping of the crystals with yttrium oxide mostly leads to increased conductivity. The maximum conductivity is inherent in 10Sc1YZr crystals.

## ACKNOWLEDGMENTS

This study was financially supported by the Russian Foundation for Basic Research (project ofi\_m no. 14-29-04081) and the Ministry of Education and Science of the Russian Federation (grant no. 14.V25.31.0018 and project no. 16.1733.2014/K).

## REFERENCES

1. Badwal, S.P.S., Ciacchi, F.T., and Milosevic, D., *Solid State Ionics*, 2000, vol. 136, p. 91.
2. Kharton, V.V., Marques, F.M.B., and Atkinson, A., *Solid State Ionics*, 2004, vol. 174, p. 135.
3. Fergus, J.W., *J. Power Sources*, 2006, vol. 162, p. 30.
4. Yokokawa, H., Sakai, N., Horita, T., Yamaji, K., and Brito, M.E., *Electrochemistry*, 2005, vol. 73, p. 20.
5. Politova, T.I. and Irvine, J.T.S., *Solid State Ionics*, 2004, vol. 168, p. 153.
6. Du, K., Kim, C.-H., Heuer, A.H., Goettler, R., and Liu, Z., *J. Am. Ceram. Soc.*, 2008, vol. 91, p. 1626.
7. Osiko, V.V., Borik, M.A., and Lomonova, E.E., *Ann. Rev. Mater. Sci.*, 1987, vol. 17, p. 101.
8. Lomonova, E.E. and Osiko, V.V., *Crystal Growth Technology*, Chichester: Wiley, 2003.
9. Osiko, V.V., Borik, M.A., and Lomonova, E.E., *Springer Handbook of Crystal Growth*, Berlin: Springer, 2010.
10. Borik, M.A., Lomonova, E.E., Osiko, V.V., Panov, V.A., Porodnikov, O.E., Vishnyakova, M.A., Voron'ko, Yu.K., and Voronov, V.V., *J. Cryst. Growth*, 2005, vol. 275, p. 2173.
11. Borik, M.A., Vishnyakova, M.A., Voitsitskii, V.P., Kulebyakin, A.V., Lomonova, E.E., Myzina, V.A., Osiko, V.V., and Panov, V.A., *Neorg. Mater.*, 2007, vol. 43, p. 1359.
12. Yashima, M., Kakihana, M., and Yoshimura, M., *Solid State Ionics*, 1996, vol. 86, p. 1131.
13. Lee, D.S., Kim, W.S., Choi, S.H., Kim, J., Lee, H.-W., and Lee, J.-H., *Solid State Ionics*, 2005, vol. 176, p. 33.
14. Abbas, H.A., Argirusis, C., Kilo, M., Wiemhöfer, H.-D., Hammad, F.F., and Hanafi, Z.M., *Solid State Ionics*, 2011, vol. 184, p. 6.
15. Omar, S., Najib, W.B., Chen, W., and Bonanos, N., *J. Am. Ceram. Soc.*, 2012, vol. 95, p. 1965.
16. Spirin, A., Ivanov, V., Nikonov, A., Lipilin, A., Parandin, S., Khrustov, V., and Spirina, A., *Solid State Ionics*, 2012, vol. 225, p. 448.
17. Nikonov, A.V., Khrustov, V.R., Bokov, A.A., Koleukh, D.S., and Zayats, S.V., *Russ. J. Electrochem.*, 2014, vol. 50, p. 625.
18. Araki, W., Koshikawa, T., Yamaji, A., and Adachi, T., *Solid State Ionics*, 2009, vol. 180, p. 1484.
19. Deryagina, I., Khrustov, V., Nikonov, A., Parandin, S., and Ivanov, V., *J. Eur. Ceram. Soc.*, 2014, vol. 34, p. 45.
20. Yuan, F., Wang, J., Miao, H., Guo, C., and Wang, W.G., *J. Alloys Compd.*, 2013, vol. 549, p. 200.
21. Fujimori, H., Yashima, M., Kakihana, M., and Yoshimura, M., *J. Am. Ceram. Soc.*, 1998, vol. 81, p. 2885.
22. Borik, M.A., Bublik, V.T., Kulebyakin, A.V., Lomonova, E.E., Milovich, F.O., Myzina, V.A., Osiko, V.V., and Tabachkova, N.Y., *J. Alloys Compd.*, 2014, vol. 586, p. 231.
23. Artemov, V.G., Kuritsyna, I.E., Lebedev, S.P., Komandin, G.A., Kapralov, P.O., Spektor, I.E., Khariton, V.V., Bredikhin, S.I., and Volkov, A.A., *Russ. J. Electrochem.*, 2014, vol. 50, p. 690.
24. Arachi, Y., Sakai, H., Yamamoto, O., Takeda, Y., and Imanishai, N., *Solid State Ionics*, 1999, vol. 121, p. 133.

Translated by L. Smolina